Surface & Coatings Technology 363 (2019) 344–351

Contents lists available at ScienceDirect

Surface & Coatings Technology

journal homepage: www.elsevier.com/locate/surfcoat

Investigation of diamond-like carbon coated steel corrosion: Enhancing the optical detection of defects by a controlled electrochemical activation

T. Maerten[a,b,*], R. Oltra[c], C. Jaoul[a], C. Le Niviven[a], P. Tristant[a], F. Meunier[b], O. Jarry[b]

[a] IRCER, UMR CNRS 7315, Université de Limoges, 87068 Limoges, France
[b] Oerlikon Balzers Coating France, 87068 Limoges, France
[c] Laboratoire ICB, UMR CNRS 6303, Université Bourgogne Franche Comté, 21078 Dijon, France

ARTICLE INFO

Keywords:
DLC
Thin film
Localized corrosion
Electrochemical test
Coated steel

ABSTRACT

It is often reported that DLC thin films have good corrosion properties due to chemical inertness and low electrical conductivity. Nevertheless, the performance of these coating is highly sensitive to the presence of growth defects. An *in situ* optical microscopy coupled to an electrochemical test was then developed to evaluate corrosion protection performance of DLC coated steel. A square wave voltammetry was applied to increase the sensitivity of electrochemical techniques based on the detection of the dissolution of the bare metal surface triggered by the presence of uncoated spots due to inherent defects. With this *in situ* electrochemical test, a clear improvement in optical detection "natural" defects is obtained. SEM coupled with FIB milling technique was used to generate artificial defects with controlled dimensions down to 2.5 µm diameter to define the sensitivity of the proposed counting procedure. Results showed that it was possible to detect cylindrical defects with diameter down to 2.5 µm. Moreover, the electrochemical approach allowed to characterize the propagation of the damage under the DLC coatings.

1. Introduction

Since almost 20 years, diamond-like carbon (DLC) thin films have been selected for tribological solutions mainly because of their excellent properties such as low coefficient of friction (five time less than bare steel in dry condition), high hardness (from 20 to 35 GPa for hydrogenated ones) and excellent wear properties (high abrasive wear resistance, preventing adhesive wear mechanisms) [1–5]. Most of the time, it has also been reported that DLC thin films have good intrinsic corrosion properties as they are chemically inert in sodium chloride solutions either in acid or basic environment [6–10]. This has led to envision and evaluate the use of DLC thin films in tribological applications that also require complementary corrosion protection performances on coated parts (for instance: in aeronautic, in food industry for mechanical devices, in automotive for non-cosmetic part of structures). Typically, these coatings are deposited on steel alloys presenting high mechanical properties, such as tool steel or bearing ring steel that demonstrate poor or limited corrosion resistance.

In an industrial context, the evaluation of corrosion protection of DLC thin films is presented, most of the time, with neutral salt spray tests or immersion tests, whereas at laboratory the evaluation would be mainly done using electrochemical techniques [9,11,12]. Recording linear sweep polarization, many authors conclude on better corrosion protection of their DLC thin films considering only the corrosion potential shift to nobler values or demonstrating the decrease of the current density without any or few considerations about defect density of the coating [9,13,14].

As illustrated, many years ago for localized corrosion studies on aluminum alloys [15], electrochemical activation of pinholes can be used to enhance their optical detection. The aim of this work was to present an electrochemical approach combined with *in situ* optical observations of the surface. Optical techniques for studying *in situ* corrosion were mainly applied to follow the propagation rate [15,16]. Recent evolution due to numerical recording (Digital Image Correlation) allowed in conjunction with Slow Strain Rate Testing has been used to explore the formation and development of local surface strain fields around localized corrosion pits for a high strength carbon steel in a seawater environment [17]. Progress in optics was also tentatively applied for describing related surface and interfacial phenomena. For example, phase detection interferometric microscopy was used to obtain high resolution surface images for pits initiating on iron in acidic solution [18]. Nevertheless, some limits in quantitative measurement could occur due to the change of refractive index in solution in presence of the corrosion products [19].

* Corresponding author at: Oerlikon Balzers, 5 Allée Skylab, 87068 Limoges, France.
E-mail address: thibault.maerten@unilim.fr (T. Maerten).

https://doi.org/10.1016/j.surfcoat.2019.02.050
Received 14 November 2018; Received in revised form 24 January 2019; Accepted 15 February 2019
Available online 16 February 2019

In this paper, we report the application of the same type of approach (at the first time to our knowledge to coating characterization) based on an electrochemical stimulation of existing defects to enhance their optical detection. To validate the efficiency of the electrochemical sequence and to define the sensitivity of the proposed approach combining cathodic and anodic potential transients, artificially created micro-defects (10 to 2.5 µm in diameter) were machined using SEM-FIB and submitted to polarization and observation.

2. Experimental

2.1. Materials

100Cr6 (AISI 52100) (A) and 90MnCrV8 (AISI O2) (B) steel were used as base metal. For (A), disk samples, 3 mm thick, were machined from a 50 mm diameter rod. Then, they were first grinded and then polished using a water based diamond suspension (12 µm) for 20 min in order to reach an average roughness of 0.05 µm. For (B), dot samples with a diameter of 22 mm were stamped from an electropolished sheet. In term of microstructure, they both exhibit a tempered martensitic structure with chromium carbides. Prior installation inside the reactor, the samples were cleaned in an industrial ultrasonic water based cleaning line.

One type of DLC coating has been tested in this paper, it was made in industrial reactors at Oerlikon Balzers combining PVD and PACVD processes. A pulsed DC power source was used for generating the plasma on the substrates. Before the deposition of the first sublayer, samples were sputter cleaned in argon plasma for 15 min at a bias voltage of −500 V. Then, sublayers were deposited using first magnetron sputtering for the titanium crystalline layer and secondly PACVD for the silicon containing amorphous layer. At last, the DLC was produced by PACVD and resulted in a hydrogenated amorphous carbon (a–C:H) coating with a hardness of 25 GPa. Coatings were deposited at a working pressure around 10^{-3} mbar. Coating architecture and thickness are summarized in Table 1.

2.2. Electrochemical set-up

For electrochemical tests, a conventional three-electrode set-up was used with a platinum counter electrode and a saturated calomel electrode (SCE) reference. All potentials are referred to SCE. Currents are given instead of current densities as it does not make sense to deal with them, because the exposed areas of steel substrate are not known due to arbitrary defects distribution for DLC coated samples. An AMETEK VersaSTAT 3 potentiostat/galvanostat was used for the measurements. The electrolyte solution was an aerated 0.1 M NaCl (Analar Normpur analytical reagent VWR BDH Prolabo) at pH 6.5 and room temperature. The exposed sample surface was limited to 4 cm^2 using O-ring. This set-up was used to perform potentiodynamic tests such as polarization curves.

2.3. In situ observation during electrochemical tests

In situ observation using digital microscope KEYENCE VHX-5000 (equipped with long range zoom lens) was coupled to the conventional electrochemical set-up presented before. In the following, this test is defined as the "*in situ* electrochemical test" and the set-up is schematically illustrated in Fig. 1. The exposed sample area was reduced to a 0.2 cm^2 disk with a PTFE adhesive mask to measure electrochemical response of single isolated defect. The experiment is also defined by the experimental polarization sequence applied to samples, it was started (and ended) with a 1 min open circuit potential (OCP) measurement to ensure system stability, and then followed by a specific potentiostatic polarization sequence. This sequence consists in a square wave polarization during which the potential of the working electrode is stepped through a series of forward and reverse pulses from −1.2 V for 1 min to +0.4 V for 1 min. This sequence was chosen to alternatively stimulate bare metal at the bottom of the small defects in anodic domain to dissolve steel and in cathodic domain, at sufficiently low potential, to reduce water in dihydrogen allowing to mechanically remove corrosion products by $H_{2(g)}$ bubbles motion. Before water reduction, at a potential close to the corrosion potential, dissolved dioxygen reduction occurs first. This sequence can be considered as an enhanced defects detection procedure using corrosion reactions.

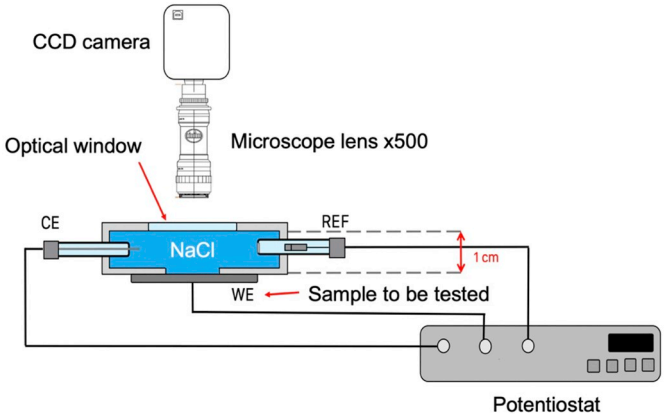

Fig. 1. Schematic diagram of the setup for the "*in situ* electrochemical test"; CE = platinum counter electrode, WE = working electrode and REF = saturated calomel reference electrode.

2.4. Complementary characterizations

To complete the *in situ* electrochemical test, the morphology of the coatings before and after corrosion tests were examined with a scanning electron microscope (SEM) ZEISS Crossbeam 550. A field ions beam (FIB) gun integrated in this SEM was used to perform nano-milling and cross-sectional views. A well-controlled thickness of material was removed from the specimen surface by sputtering. A Ga^+ beam was employed at 30 kV and 15 nA to mill the sample. Then, to obtain a smooth and well-polished cross section, the final milling step was performed at 30 kV and 700 pA. An energy-dispersive analysis by X-rays (EDAX) microprobe was also coupled to SEM to carry out the chemical analysis of these cross sections. They were performed with a 5 kV electron beam. Additional cross-sectional views and analysis have been performed using Ar^+ ion polishing device GATAN 691 PIPS and a standard ZEISS SEM coupled with EDAX microprobe.

Table 1
Architecture and thickness of the coating developed by Oerlikon Balzers.

Sublayer 1 (from substrate)	Sublayer 2	Top layer	Total thickness
Titanium by magnetron sputtering (~0.40 µm)	Ceramic-like amorphous layer containing silicon (~0.85 µm)	a–C:H DLC layer (~1.0 µm)	~2.5 µm

3. Results and discussion

3.1. Morphology of DLC coating surface: origin of defects

Before any electrochemical activation, observations of steel (A) coated with DLC surface were performed using digital microscope and SEM coupled with EDAX microprobe. They revealed some macro defects with diameters sizes in the range of 10 to 60 µm (Fig. 2). An EDX map of one of them for C, Si, O, Ti and Fe showed that the bottom of the defect was clearly the uncoated steel surface (Fig. 3). The main origin of

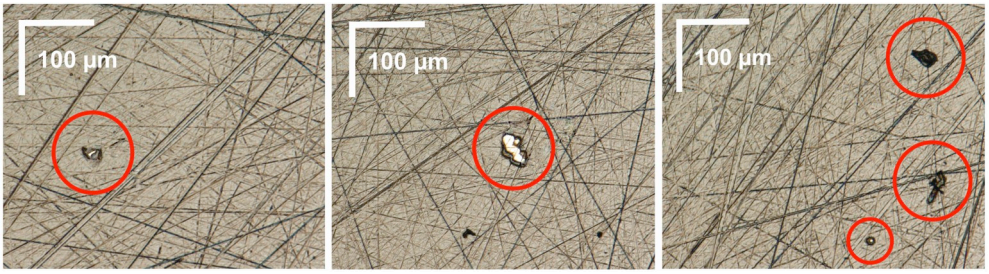

Fig. 2. Typical defects due to the presence of dusts particles (substrate roughness Ra = 0.05 µm).

these defects, resulting in the absence of the coating, are mostly due to micrometric dust particles present on the substrate before deposition or generated during deposition due to rotation of substrate holder, micro-arcing [20]. Fenker *et al.* have detailed such defects in PVD hard coatings responsible of corrosion attack of the substrates in their review [21]. In case of immersion, the mouth of these macro defects will represent a critical path for the electrolyte which can reach the metal surface at their bottoms.

3.2. Electrochemical experiments on DLC coated steel

3.2.1. Approach based on the mixed potential theory

As indicated in a previous paper [12], the mixed potential concept or the method of polarization curves superposition was found to be more suitable to define the defect density of the coated metal. Typical polarization measurements, imposing a linear sweep voltammetry, have been recorded from −1 V to +1 V at a sweep rate of 0.5 mV/s on bare steel (A) and steel (A) coated with DLC (Fig. 4). Fig. 4a represents the plot of a polarization curve in a logarithm scale while Fig. 4b represents it in linear scale for current. Logarithm scale representation allows to clearly define the mixed corrosion potentials. Below this corrosion potential, is the cathodic domain where dioxygen reduction happens and above it, is the anodic domain where dissolution of steel occurs. For both samples, this corrosion potential is around −0.5 V and −0.4 V indicating substrate metal in contact with electrolyte. Regarding curves of uncoated and coated samples in Fig. 4a, it can be deduced that DLC acts as barrier against electrolyte as the current is 3 orders of magnitude lower in cathodic domain for the coated sample.

Assuming the recorded current on coated samples is the cumulative value of the currents inside the coating defects, the equivalent defected surface could be, *a priori*, estimated by the ratio of the current in the anodic (dissolution current) or cathodic (dioxygen reduction current) domains. But in the cathodic domain, because the cathodic current is under the control of dioxygen diffusion it was impossible to use this approach because the diffusion regime inside the localized defects corresponded more to the regime observed for ultra-microelectrodes [22] than the regime of diffusion observed for the flat surface of the bare metal electrode. Moreover, the nature of metal exposed at defect bottom is not clearly defined. Indeed, the presence of a titanium layer

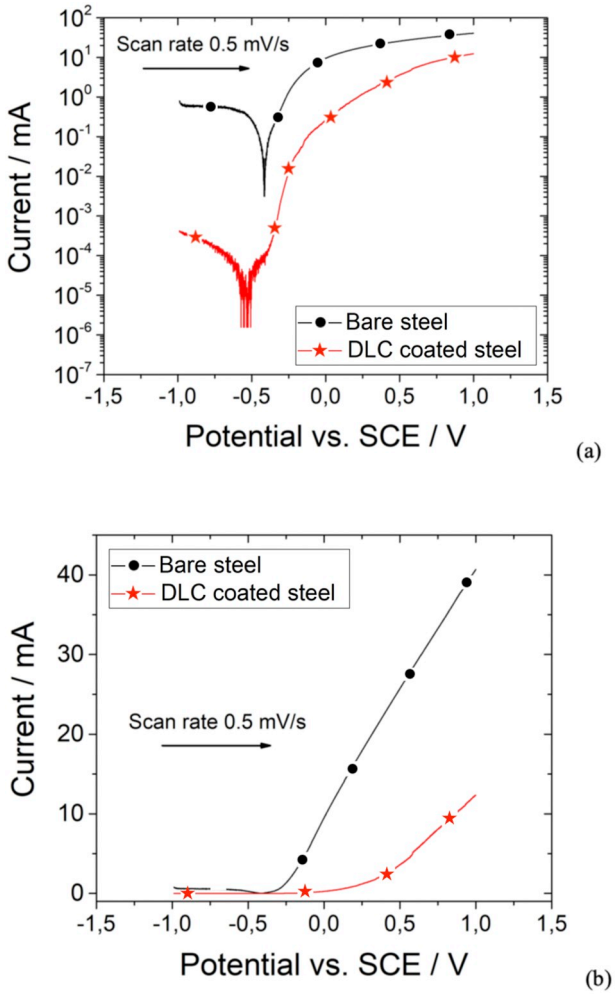

Fig. 4. Polarization curves for a bare and coated with DLC 100Cr6 steel plotted in logarithm current scale (a) and in linear current scale (b).

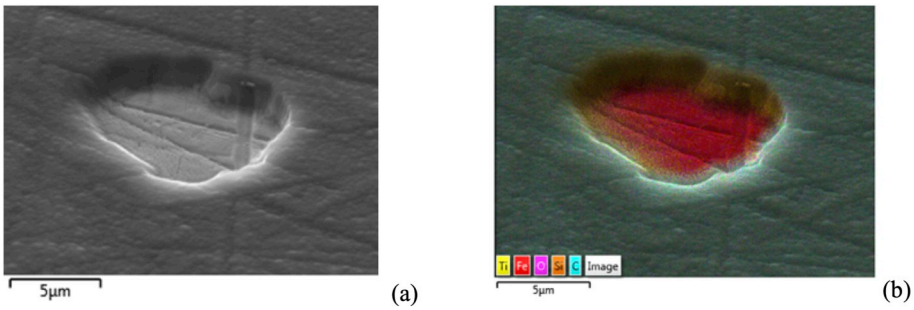

Fig. 3. (a) SEM and (b) chemical analysis (EDAX) of the surface of a 10 µm diameter defect in a DLC coating (same conditions than in Table 1).

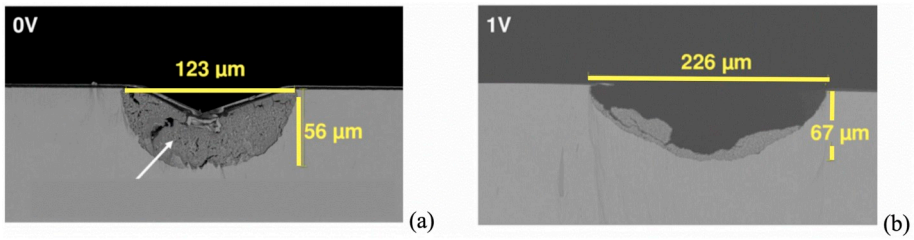

Fig. 5. SEM cross-sections of corrosion attack triggered by an isolated defect. The polarization was stopped at 0 V (a) and 1 V (b). (a): the white arrow indicated the location of some undissolved chromium carbides.

can affect the cathodic reduction of dissolved oxygen by modifying the reaction kinetics and consequently the corrosion potential deduced on the polarization curve on the coated specimen.

Regarding the anodic domain, as shown in Fig. 4b, the ratio between the currents measured on the bare and coated samples are not proportional along the recording of the polarization curve. This can be explained by the time dependence of the growth of the corroding defects, *e.g.* the corroding surface is increasing as function of time as it will be illustrated in Fig. 5. On the other hand, the ohmic control of the anodic current variation, as shown in Fig. 4b for large overpotentials, does not correspond to the same physical control on bare metal compared to coated specimen. On bare metal the ohmic effect is due to the location of the reference electrode (a Luggin capillary was not used) whereas in the case of DLC coated specimens the anodic current is flowing through localized defects which induce an ohmic resistance. Moreover, this defect resistance which would be of interest to quantify the size of the defect is varying as function of time, as already mentioned.

To summarize, the polarization curve plotted on the coated substrate presenting some defects cannot be considered to be proportional to the one plotted on the bare metal surface, assuming that the exposed corroding surface of the coated sample is represented by the cumulative surface of the defects where the metallic substrate is in contact with electrolyte.

3.2.2. Analysis of the propagation of a defect

To clarify the origin of these limitations, especially in the anodic domain, two pinholes have been observed from two separate specimens coated with DLC and polarized in the same conditions than in Fig. 4. Polarization measurements were both started at −1 V but stopped for one at 0 V and the other at 1 V in order to be able to observe first stage of corrosion attack under coating. As shown the cross section in Fig. 5, two different morphologies were observed. At 0 V under the coating a hemispherical occluded cavity closed by the remaining DLC film was observed. This cavity was full of corrosion products resulting from dissolution of the steel matrix. This lead to the formation of a sponge-like structure representing the corrosion products which cannot be released from the cavity due to the small aperture (the initial defect) in the cover (Fig. 5a). It is worth noticing that inside these entrapped corrosion products chromium carbides remaining from the initial microstructure of the steel, can be detected.

After polarization at 1 V, the coating on top of the cavity and the sponge-like corrosion products are no longer observed on the cross section presented in Fig. 5b. An empty hemispherical cavity of 226 µm diameter and 67 µm depth is in direct contact with the electrolyte solution. An anisotropic oxidation can be noticed. The fact that the cavity seems to propagate further in the lateral direction (Fig. 5a) can be explained by results obtained in previous works on pit propagation [23]. This feature is controlled by the current distribution along the walls of the cavities and is enhanced, in our example, by the presence of the sponge-like corrosion products confined in the cavity covered by the remaining mechanical resistant DLC coating which enhances the diffusion control of the anodic dissolution [24].

The change in the corrosion regime as observed in Fig. 5b, is probably due to an uncontrolled mechanical breakdown of the DLC cover due to the stresses generated by the Pilling–Bedworth ratio of the corrosion products (mainly hydroxides) combined with compressive stresses of DLC layer. Regarding the detection of defects (counting) the surface aspect representing an open cavity (Fig. 5b) is more suitable because optical detection will be easier. To improve the control of the removal of the DLC cover from the top of cavities induced by the underneath dissolution of metallic substrate, the already described square wave polarization sequence was applied in the following part.

3.3. Enhanced optical defects detection during electrochemical experiments on DLC coated steel

3.3.1. Electrochemical response of existing defect in DLC coatings

From results described in Fig. 5 it appears that anodic polarization will induced a more efficient effect in terms of defect detection. In the following experiment, a controlled and limited electrochemical activation of existing defects using the *in situ* electrochemical set up (described in Fig. 1) were performed. The number of existing defects could be estimated by optical observations.

Some of dust defects, observed in Fig. 2, were isolated using a PTFE mask and *in situ* electrochemical tests were performed on a small area with only one visible defects. For example, a coated specimen with a single 20 µm diameter defect is displayed in Fig. 6a and it is compared with a DLC coated surface free of defects (Fig. 6b). While monitoring the surface with the microscope, the current transient responses were recorded during the application of the square wave potential alternating anodic and cathodic potential as described in experimental part. In the case of a surface with one defect, optical and current detection are correlated. At t = 390 s, an activity inside the defect is optically detectable and a current transient is measured in this anodic step. In the case of defect-free surface, no current change is observed as well as surface degradation (Fig. 6b). With this *in situ* electrochemical test, a clear improvement in optical defects detection is achieved. Even if this *in situ* approach is more efficient to detect the existing defects on a DLC coating, only a counting of these defects is possible without an access to their initial size distribution.

To validate this first step, the sensitivity of the approach has been tentatively checked. To define the critical threshold value of the defect diameter to be detected by this *in situ* electrochemical test, defects were artificially machined using SEM coupled with FIB to perform nano-milling inside the coating. Shape controlled (cylindrical holes) defects with various diameters from 20 µm down to 2.5 µm were milled on well-defined locations on a defects-free zone.

3.3.2. Electrochemical response of an artificially defect machined in DLC coatings

In this section, the objective was to determine until which size of defects, corrosion can occur and is detected by the digital microscope. Only the case of the smaller artificial defect, with a diameter of 2.5 µm, is presented. To mill these artificial defects into DLC coating, FIB was set to 30 kV and 7 nA (instead of 14 nA like for cross section

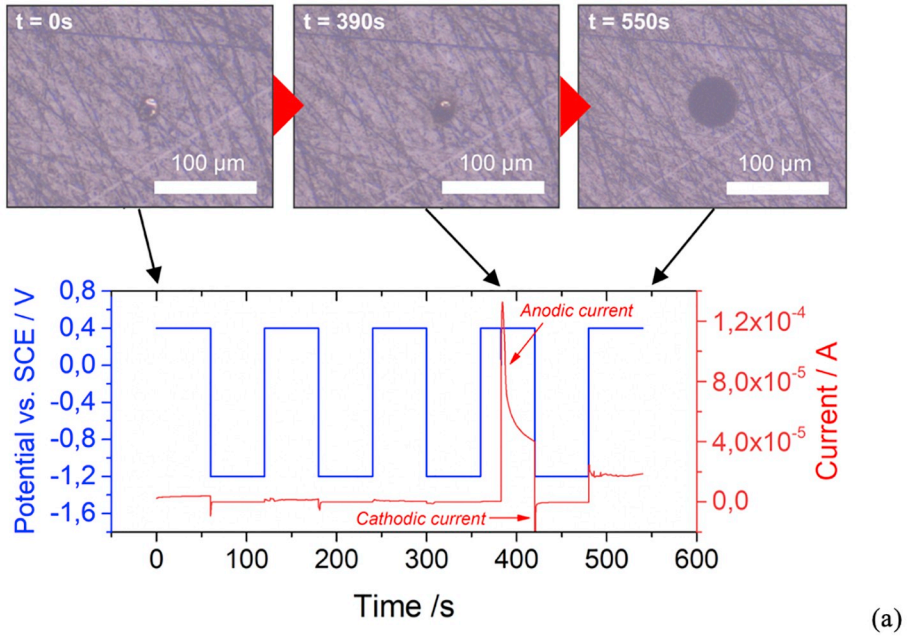

Fig. 6. *In situ* temporal series of microscope imaging coupled with electrochemical activation induced by a pulse sequence cycling the potential from a cathodic (1 min) to an anodic (1 min) value. (a) For a "real" defect. (b) For an undamaged surface. Both working electrodes are steel coated with a DLC based coating.

preparation) to reach the desired geometry. Cross section of them was performed to control their cylindrical shape and be sure that they reach the substrate (Fig. 7).

The DLC coating used to perform these artificial defects consisted of a double stack of the DLC coating presented in experimental section; the titanium layer was only deposited on substrate not on the DLC intermediate layer. To summarize, the coating architecture was Ti (0.3 µm)/Si-sublayer (0.8 µm)/DLC (1 µm)/Si sublayer (0.8 µm)/DLC (1 µm). This double stack of the DLC was used instead of single stack DLC coating to limit the presence of "natural" defects and therefore to be sure to only record the current from the artificial defect. A position mark was milled in depth of coating for only few nanometers in order to be able to locate easily the defect in the 0.4 cm^2 surface (Fig. 8). Substrate used in this case was steel (B) due to its mirror-like surface polishing enabling to clearly choose and locate milled defects.

After milling the defect, the 0.4 cm^2 surface was exposed to the electrolyte and the *in situ* electrochemical test was performed. Fig. 8a and b presents *in situ* imaging of the surface before (at t = 0 s) and after (at t = 150 s) the test. Corrosion products (orange rust: $Fe(OH)_2$) were observed around the defect location. Corrosion products were expelled during the cathodic phases of the test by H_2 bubbles release which acts as mechanical cleaning of the cavity. Also, the related current resulting from electrochemical reaction was recorded (Fig. 8c). The test was stopped after third anodic potential squares in order to avoid a too large damage of the sample. During the first anodic cycle of the imposed square wave potential, no activity was recorded but on the second one,

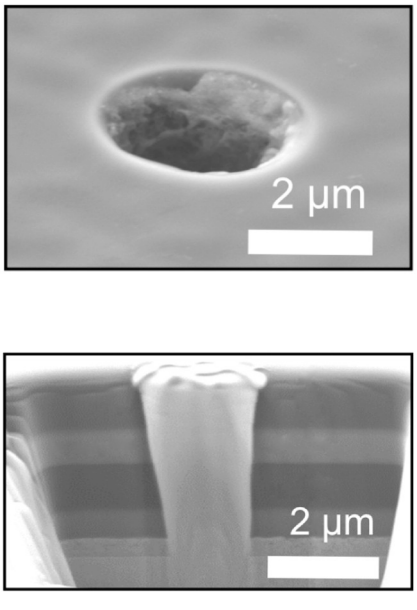

Fig. 7. SEM top surface (a) and cross-sectional (b) views of a 2.5 µm diameter artificial defect produced by FIB machining.

a constant 0.75 µA current was recorded. The current (negative) related to the reduction was slightly lower around −0.05 µA constant current. The current recorded for the third anodic cycle was much lower at 0.1 µA. This could be explained by diffusion phenomenon occurring inside the pit. These results demonstrate that a single 2.5 µm diameter defect in the DLC coating can be detected by following the current response in the range of few hundreds of nA. On the same kind of

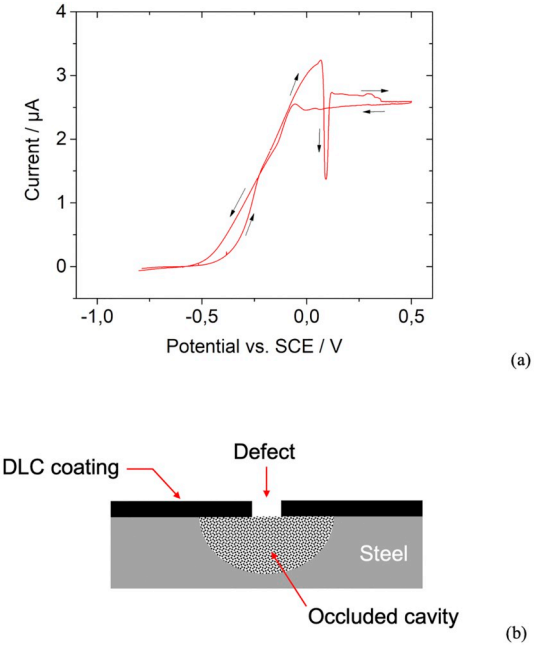

Fig. 9. Characteristics of an artificial propagating defect. (a) Current-voltage curve. (b) Schematic geometrical description of the growing defect.

triggering artificial defect it was easier to validate some assumptions (see 3.2.3) about the dissolution mechanism involved during the damage propagation underneath the remaining DLC layer.

On the previously selected artificial defect already active, a cyclic polarization was carried out from −0.8 V to 0.5 V and reverse to −0.8 V (Fig. 9a). From the corrosion potential (approx. −0.5 V)

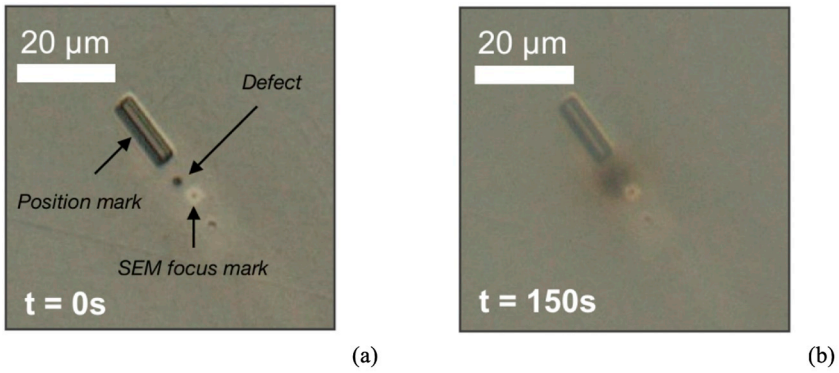

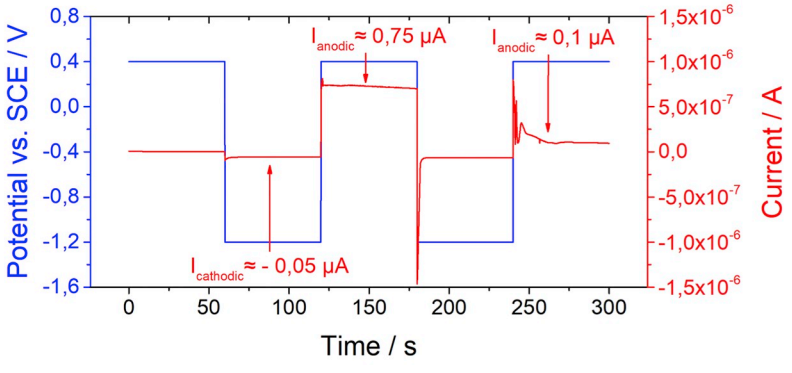

Fig. 8. Electrochemical activation of an artificial defect. (a) Initial defect (t = 0 s). (b) Induced damage after one potential cycle (t = 150 s). (c) Imposed pulse sequence cycling the potential from a cathodic (1 min) to an anodic (1 min) value and recorded current.

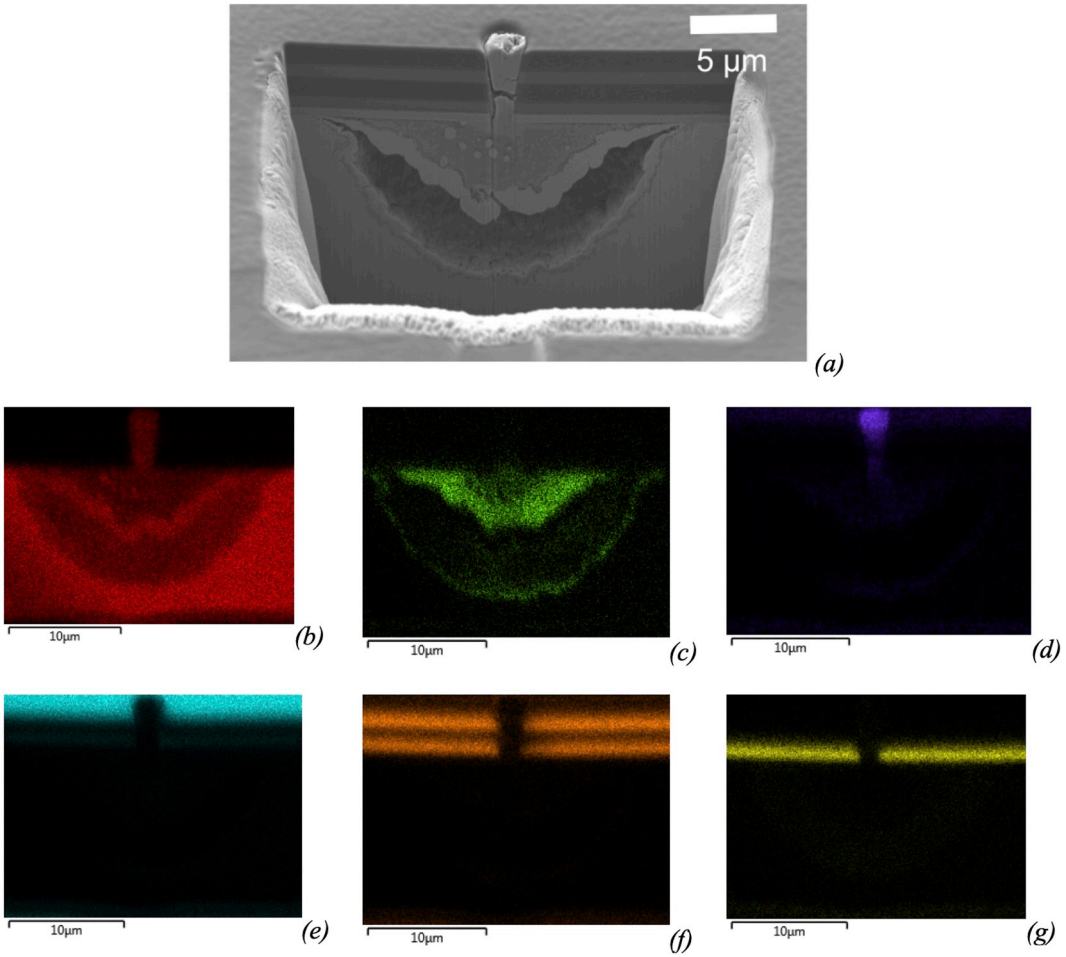

Fig. 10. SEM observation and chemical composition map analysis of a cross-section obtained on a 2.5 µm diameter artificial defect produced using FIB and after "in situ electrochemical test". (a): Internal morphology of the cavity due to the propagation of the corrosion underneath the DLC coating. (b) to (g): EDX map analysis respectively for Fe, Cl, O, C, Si and Ti.

current increases linearly until +0.1 V where a current drop is observed, the current value is then stabilized around 2.5 µA as potential still steps up. On the reverse scanning, the current value remains constant till a potential of −0.1 V where current decreases linearly with the same initial slope. Following the electrochemical test, a cross sectional view was carried out to observe the corrosion attack under the coating where the defect was generated (Fig. 10a), also EDX map analysis were done on selected elements Fig. 10b to g). Chemical composition of the surface shows the remaining DLC coating (Fig. 10e to g). But, dioxygen is only present and linked to iron at the mouth of the initial defect on the coating (Fig. 10b and d). It confirms some modelling approach showing that $Fe(OH)_2$ will be present at the mouth [25].

The recorded current exhibits a typical time profile which confirms the transition between two controlling regimes. On the current-voltage curve (Fig. 9a), in the forward direction the current increases linearly (Ohmic control), this leads to the dissolution of the metallic interface inside the cavity (Fig. 9b) in which the solution reaches a supersaturated concentration level at the current peak. At this maximum, a salt film is formed. This salt film has been detected on EDX analysis presented in Fig. 10b and c and it consists of $FeCl_2$ and as a consequence the rate of dissolution is lowered. After this transition, the current remains constant because it is under mass transport control. On the reverse sweep the salt film will thinned and then completely dissolved. This feature was first detected by other authors for a 1D artificial pit consisting of an iron or stainless-steel wire embedded in a resin [26]. It is for the first time at our knowledge that the same feature can be reproduced following the propagation of a well-defined 3D cavity. This result illustrates the controlling mechanisms involved in the propagation of a localized defect in a DLC coating and can be used to model the risk of damage which can affect coated specimens.

Regarding the initial objective of this work, the analysis (counting) of existing defects, the electrochemical activation combined with an *in situ* optical microscopy allows to detect defect smaller than few micrometers in diameter (a minimum value of 2.5 µm leads to a detectable signal).

4. Conclusion

An *in situ* optical microscopy coupled to an electrochemical activation based on a variant of the Square Wave Voltammetry was developed to increase the sensitivity of electrochemical techniques based on the detection of the dissolution of the bare metal surface triggered by the presence of uncoated spots. The voltage cycle imposed to the coated working electrode, lower potential and upper potential, was chosen to promote at short time during the cycling an open cavity which can be clearly optically detected. With this *in situ* electrochemical test, a clear improvement in optical detection of "natural" defects was obtained. SEM coupled with FIB milling technique was used to generate artificial defects down to 2.5 µm diameter to define the sensitivity of the proposed counting procedure. Beyond the main purpose of this work, the electrochemical approach allowed to characterize the limiting processes of the propagation of the damage located in front of sensitive microscopic apertures existing inside the coating. The shape of the induced damage to the underneath iron based alloy will always be an

occluded hemispheric cavity resulting from the dissolution of the metallic substrate controlled by mass transport and limited by the precipitation of metallic chlorides.

Acknowledgements

This work was financially supported by ANRT (Agence Nationale de la Recherche et de la Technologie). The authors would like to thank P. Duport (IRCER) for performing the different SEM FIB millings and cross-sections and J. Fougeyrollas (CITRA) for ions polishing and SEM observations.

References

[1] C. Donnet, A. Erdemir, Tribology of Diamond-like Carbon Films, Springer, Boston, MA, 2008, pp. 1–673.
[2] A. Grill, Diamond-like carbon: state of the art, Diam. Relat. Mater. 8 (1999) 428–434.
[3] K. Bewilogua, D. Hofmann, History of diamond-like carbon films — from first experiments to worldwide applications, Surf. Coat. Technol. 242 (2014) 214–225.
[4] J. Robertson, Diamond-like amorphous carbon, Mater. Sci. Eng. 37 (2002) 129–281.
[5] O. Jarry, C. Jaoul, P. Tristant, T. Merle-Méjean, M. Colas, C. Dublanche-Tixier, H. Ageorges, C. Lory, J.-M. Jacquet, Tribological behaviour of diamond-like carbon films used in automotive application: a comparison, Plasma Process. Polym. 6 (2009) 478–482.
[6] R. Sharma, P.K. Barhai, N. Kumari, Corrosion resistant behaviour of DLC films, Thin Solid Films 516 (2008) 5397–5403.
[7] R.P.O.S. Nery, R.S. Bonelli, S.S. Camargo, Evaluation of corrosion resistance of diamond-like carbon films deposited onto AISI 4340 steel, J. Mater. Sci. 45 (2010) 5472–5477.
[8] E.L. Dalibón, M.A. Guitar, V. Trava-Airoldi, F. Mücklich, S.P. Brühl, Plasma nitriding and DLC coatings for corrosion protection of precipitation hardening stainless steel, Adv. Eng. Mater. 18 (2015) 826–832.
[9] Z. Wang, C. Wang, Q. Wang, J. Zhang, Electrochemical corrosion behaviors of a-C:H and a-C:Nx:H films, Appl. Surf. Sci. 254 (2008) 3021–3025.
[10] H. Miya, J. Wang, Corrosion protect DLC coating on steel and Hastelloy, Mater. Trans. 49 (2008) 1333–1337.
[11] M.A.S. Oliveira, M. Massi, L.N. Nishioka, G.P. Thim, R.W. Bartar, A.K. Vieira, Efficiency of diamond-like carbon films on corrosion protection of titanium alloys, J. New Mater. Electrochem. Syst. 5 (2002) 67–70.
[12] J. Creus, H. Mazille, H. Idrissi, Porosity evaluation of protective coatings onto steel, through electrochemical techniques, Surf. Coat. Technol. 130 (2000) 224–232.
[13] S. Guruvenket, M. Azzi, D. Li, J.A. Szpunar, L. Martinu, J.E. Klemberg-Sapieha, Structural, mechanical, tribological, and corrosion properties of a-SiC:H coatings prepared by PECVD, Surf. Coat. Technol. 204 (2010) 3358–3365.
[14] S.-S. Hadinata, M.-T. Lee, S.-J. Pan, W.-T. Tsai, C.-Y. Tai, C.-F. Shih, Electrochemical performances of diamond-like carbon coatings on carbon steel, stainless steel, and brass, Thin Solid Films 529 (2013) 412–416.
[15] Clive D.S. Tuck, Use of video techniques to study the electrochemical activation and corrosion of aluminium alloys, Faraday Discuss. 94 (1992) 171–182.
[16] A.-M. Zimer, M.A.S. De-Carra, L.-H. Mascaro, E.C. Pereira, Temporal series of micrographs coupled with electrochemical techniques to analyze pitting corrosion of AISI 1040 steel in carbonate and chloride solutions, Electrochim. Acta 124 (2014) 143–149.
[17] P.E. Barnes, S.B. Lyon, D.L. Engelberg, In-situ surface strain mapping of pitting corrosion in a high strength carbon steel, Eurocorr (2014) Pisa, Italy, Paper 7226.
[18] H.J. Kragt, D.J. Earl, J.D. Norton, H.S. White, Phase detection interferometric microscopy of electrode surfaces. Measurement of localized dissolution of iron electrodes, J. Electrochem. Soc. 136 (1989) 1752–1755.
[19] C.P. Smith, D.C. Fritz, M. Tirrell, H.S. White, Phase measurement interferometric microscopy of thin films: analysis of topography, refractive index, and thickness of solvent swollen polystyrene films, Thin Solid Films 198 (1991) 369–386.
[20] P. Panjan, P. Gselman, D. Kek-Merl, M. Čekada, M. Panjan, G. Dražić, T. Bončina, F. Zupanič, Growth defect density in PVD hard coatings prepared by different deposition techniques, Surf. Coat. Technol. 237 (2013) 349–356.
[21] M. Fenker, M. Balzer, H. Kappl, Corrosion protection with hard coatings on steel: past approaches and current research efforts, Surf. Coat. Technol. 257 (2014) 182–205.
[22] Allen J. Bard, Larry R. Faulkner, Electrochemical Methods Fundamentals and Applications, John Wiley & Sons, Inc., 2001, p. 168.
[23] S.M. Ghahari, D.P. Krouse, N.J. Laycock, T. Rayment, C. Padovani, T. Suter, R. Mokso, F. Marone, M. Stampanoni, M. Monir, A.J. Davenport, Pitting corrosion of stainless steel: measuring and modelling pit propagation in support of damage prediction for radioactive waste containers, Corros. Eng. Sci. Technol. 46 (2011) 205–221.
[24] N.J. Laycock, S.P. White, Computer simulation of single pit propagation in stainless steel under potentiostatic control, J. Electrochem. Soc. 148 (2001) B264–B275.
[25] S. Tricoit, Modélisation et simulation numérique de la propagation de la corrosion par piqûres du fer en milieu chloruré: Contribution à l'évaluation de la durabilité des aciers au carbone en conditions de stockage géologique, thesis University of Burgundy, 2012.
[26] J. Soltis, D. Krouse, N. Laycock, Localised dissolution of iron in buffered and non-buffered chloride containing solutions, Corros. Sci. 53 (2011) 2152–2160.